DOI 10.1007/s11141-019-09935-4
Radiophysics and Quantum Electronics, Vol. 61, No. 10, March, 2019
(Russian Original Vol. 61, No. 10, October, 2018)

CHAOTIC DYNAMICS AND MULTISTABILITY IN THE NONHOLONOMIC MODEL OF A CELTIC STONE

A. S. Gonchenko,[1], S. V. Gonchenko,[1]
A. O. Kazakov,[2,1*] and E. A. Samylina[2,1]

UDC 517.925+517.93

We study dynamic properties of a Celtic stone moving along a plane. We consider two-parameter families of the corresponding nonholonomic models in which bifurcations leading to changing the types of stable motions of the stone, as well as the chaotic-dynamics onset are analyzed. It is shown that the multistability phenomena are observed in such models when stable regimes of various types (regular and chaotic) can coexist in the phase space of the system. We also show that chaotic dynamics of the nonholonomic model of a Celtic stone can be rather diverse. In this model, in the corresponding parameter regions, one can observe both spiral strange attractors of various types, including the so-called discrete Shilnikov attractors, and mixed dynamics, when an attractor and a repeller intersect and almost coincide. A new scenario of instantaneous transition to the mixed dynamics as a result of the reversible bifurcation of merging of the stable and unstable limit cycles is found.

1. INTRODUCTION

Celtic stone is a solid which has a round symmetric surface, but with dynamic asymmetry. The latter property is already manifested in the simplest experiments as follows. If such a stone is placed on an even surface and rotated round its vertical axis in a certain direction, e.g., counterclockwise, it can steadily continue its rotation as any round body. However, if we try to rotate this stone clockwise, it slows down, starts to rock strongly, reverses its motion, and, finally, continues its steady counterclockwise rotation without any obvious cause. [1]

The strange behavior of Celtic stones and their reverse rotation have remained unexplained for many years. Various erroneous explanations of this effect are related to the features of an internal structure of the Celtic stone, special properties of the friction forces emerging during the stone rotation, Earth's rotation around its axis, etc.

An English physicist Gilbert Thomas Walker, who presented a certain physical explanation of the observed phenomena in [2], was one of the first (in late XIXth century) scientists who started to study Celtic stones from the scientific viewpoint. An American physicist Jearl Walker presented several types of Celtic stones (some of them are shown in Fig. 1) and offered a detailed description of possible motions of each stone in 1979 in [3].

A truncated paraboloid with a massive rod fixed at the geometric center of the section (see Fig. 2) can conveniently be considered as a geometric model of the Celtic stone. If there is full symmetry of the

* kazakovdz@yandex.ru

[1] The stones with such dynamic properties have been known for a very long time. Even ancient Celts used these stones apparently for cultic purposes to demonstrate divine powers. The Celtic stone has many other names, e.g., anagyre, celt, rebellious celt, rattleback, rattlerock, spin bar, wobble stone, etc. See [1] for more detail.

[1] N. I. Lobachevsky State University of Nizhny Novgorod; [2] Higher School of Economics, Nizhny Novgorod, Russia. Translated from Izvestiya Vysshikh Uchebnykh Zavedenii, Radiofizika, Vol. 61, No. 10, pp. 867–882, October 2018. Original article submitted July 9, 2018; accepted October 28, 2018.

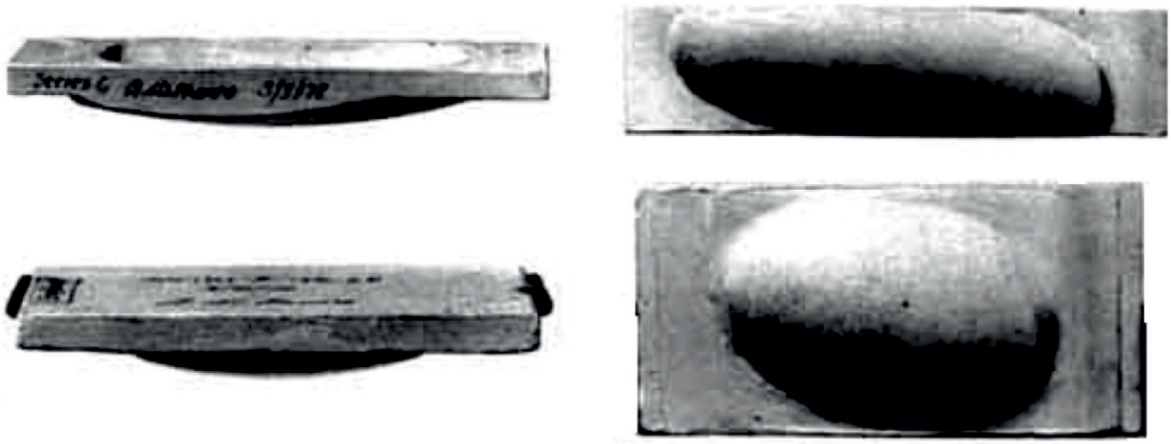

Fig. 1. Celtic stones described by J. Walker in [3].

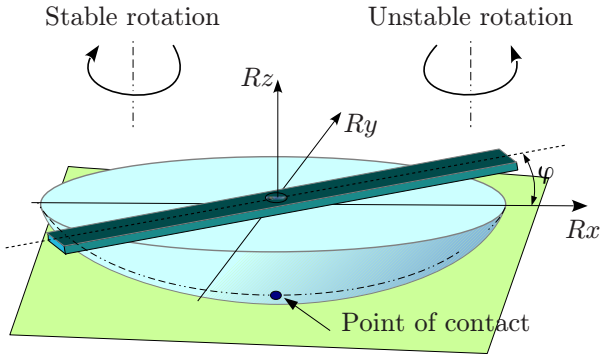

Fig. 2. Geometric model of the Celtic stone. The main body is a truncated paraboloid extended along one of the horizontal axes (the Rx axis) and compressed along the other horizontal axis (the Ry axis). The body has a horizontal area with a sufficiently massive rod fixed at the geometric center of this area. This rod can be rotated in the area plane, thereby creating a certain dynamic asymmetry.

mass location in this stone where, e.g., the rod axis is aligned with the Rx or Ry axis (i.e., $\varphi = 0$ or $\varphi = \pi/2$, respectively), the reverse phenomenon is absent. However, it immediately appears once $0 < \varphi < \pi/2$, and the rotation is rather fast.

According to J. Walker, the "actual" Celtic stone should have the following properties.

1. Dynamic asymmetry. One of the main inertia axes of the stone is vertical, while the two horizontal inertia axes should be rotated to a certain angle with respect to the geometric symmetry axes of the stone surface. In this case, the main horizontal moments of inertia of the stone should be different.

2. Geometric asymmetry. The stone surface should be boat-shaped, i.e., the curvature radii of its surface should be different at the point of contact with the support plane.

In this work, we study the nonholonomic models of the Celtic-stone motion along the plane. Such models were studied in many works. Thus, Astapov [4], Karapetyan [5], and Markeev [6] were among the first who studied the issues of stability of the stone dynamics and clarified that the dynamic asymmetry of the Celtic stone is the main cause of its reverse motion. [2] The existence of chaotic dynamics in the nonholonomic model of Celtic stone has been recently discovered in [7] in which it is shown that strange attractors can emerge in the model (see also [8–10]). In our works [11, 12], it was shown that not only strange attractors can appear, but also the mixed dynamics can be observed in this model, along with the discrete Lorenz attractors which can exist in some Celtic-stone models [13, 14]. Recall that the mixed dynamics is the new, recently discovered third type of dynamical chaos (along with the strange attractors and conservative chaos), which is characterized by the fact that an attractor and a repeller intersect and almost coincide [16]. This type of chaos is, in particular, characteristic of nonconservative systems [17–19],

[2] Geometric asymmetry is also important. For example, it distinguishes between the Celtic stone and the Chaplygin top which is sphere-shaped, but has dynamic asymmetry because of the nonuniform mass distribution. The reverse phenomenon has recently been observed in this model as well [15].

which are reversible in time. The majority of nonholonomic models of motion of solids belong to this class and, therefore, it is not surprising that they often demonstrate mixed dynamics (see, e.g., [12, 20–22]).

This article has the following structure. The nonholonomic model of a Celtic stone is presented in Sec. 2 using the system of ordinary differential equations. The main results of this work are given in Sec. 3, which contains a bifurcation analysis in the case of two-parameter families. As natural control parameters, we consider the value of the total energy $\mathcal{H}$ of the stone (this parameter is denoted by E) and the dynamic-asymmetry angle δ.[3] From physical considerations, it is obviously sufficient to consider the angle δ in the range from 0 to $\pi/2$. In this work, the main attention is paid to the issues of stability of dynamics in the nonholonomic model of Celtic stone. We elucidate the main bifurcations, which are related to both appearance of the stable (stationary, periodic, and chaotic) regimes and their disappearance.

In Sec. 4, these bifurcations are explained in the context of one-parameter families with the parameter E for the fixed angle δ. We consider three cases, namely, $\delta = 0.2$, $\delta = 0.6$, and $\delta = 1$. In Sec. 5, we discuss multistability of the Celtic-stone dynamics, i.e., the phenomenon for which the stable regimes of various types (regular–regular, regular–chaotic, and chaotic–chaotic) coexist in the phase space of the system.

2. NONHOLONOMIC MODEL OF A CELTIC STONE

2.1. Equations of motion

To study the dynamic properties of a Celtic stone, one should have an adequate mathematical model describing its motions. The so-called nonholonomic model, which is based on the assumption that the sliding is absent during the stone motion (rotation and rolling) on the plane, is the most widespread and simplest in a certain sense. If the vectors of the angular velocity and the velocity of the center of mass of the stone are denoted by $\boldsymbol{\omega}$ and $\boldsymbol{v}$, respectively, and the vector connecting the center of mass of the stone with the contact point is denoted by $\boldsymbol{r}$ (see Fig. 3), then the condition of the sliding absence during the stone motion has the form

$$\boldsymbol{v} + \boldsymbol{\omega} \times \boldsymbol{r} = 0.$$

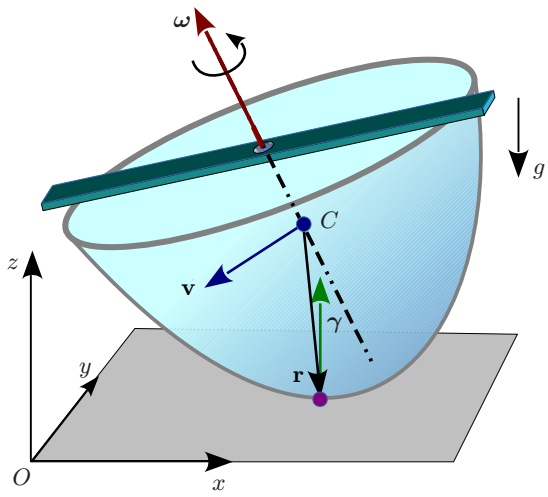

Fig. 3. Celtic stone on the plane. The main vectors.

Hereafter, all the vectors are written in the moving coordinate system, which is rigidly connected with the body and has its origin at the center of mass so that the coordinate axes coincide with the main axes of inertia of the body. As distinct from this system, the absolute coordinate system $Oxyz$ is rigidly connected with the supporting plane.

To develop the nonholonomic model, one should use the well-known laws of mechanics, namely, the law of conservation of momentum and the law of conservation of angular momentum. The final system consists of six differential equations [7]

$$\dot{\mathbf{M}} = \mathbf{M} \times \boldsymbol{\omega} + m\dot{\mathbf{r}} \times (\boldsymbol{\omega} \times \mathbf{r}) + mg\,\mathbf{r} \times \boldsymbol{\gamma}; \qquad \dot{\boldsymbol{\gamma}} = \boldsymbol{\gamma} \times \boldsymbol{\omega}, \tag{1}$$

which characterize variations in the moments of inertia $\mathbf{M} = (M_1, M_2, M_3)$ and orientation $\boldsymbol{\gamma} = (\gamma_1, \gamma_2, \gamma_3)$ of the Celtic stone (see Fig. 3). Here, the vector $\mathbf{M}$ and the angular-velocity vector $\boldsymbol{\omega}$ are related as follows:

[3] Note that the angles δ and φ (see Fig. 2) differ in the general case, namely, φ is the angle between the Ox axis and the rod axis, δ is the angle between the Ox axis and the corresponding horizontal axis of inertia. They coincide if $\varphi = 0,\ \pi/2$, or in the "nonphysical case" where the mass of the main body equals zero, i.e., its entire mass is concentrated in the rod.

$$\mathbf{M} = \mathbf{I}\boldsymbol{\omega} + m\mathbf{r} \times (\boldsymbol{\omega} \times \mathbf{r}), \tag{2}$$

where $\mathbf{I} = \mathrm{diag}(I_1, I_2, I_3)$ is the inertia tensor and the vector $\mathbf{r}$ is a function of the angle δ and the stone-surface shape. For example, in the case of a Celtic stone shaped as a truncated paraboloid, it is assumed that $\mathbf{r} = \mathbf{Q}\mathbf{r}^*$, where

$$\mathbf{Q} = \begin{pmatrix} \cos\delta & \sin\delta & 0 \\ -\sin\delta & \cos\delta & 0 \\ 0 & 0 & 1 \end{pmatrix}$$

is the matrix of rotation between the main horizontal inertia axes and the geometrical axes of the paraboloid, and the components of the vector $\mathbf{r}^*$ are related to the components of the vector $\boldsymbol{\gamma}$ by the formulas

$$r_1^* = -a_1\frac{\gamma_1}{\gamma_3}, \;\; r_2^* = -a_2\frac{\gamma_2}{\gamma_3}, \;\; r_3^* = -\tilde{h} + \frac{a_1\gamma_1^2 + a_2\gamma_2^2}{2\gamma_3^2}, \tag{3}$$

in which a_1 and a_2 are the main curvature radii of the paraboloid and $\tilde{h}$ is the height of the center of mass of the stone.

Note that using Eqs. (2) and (3), we can rewrite system (1) in closed form. Indeed, since $\mathbf{r} = \mathbf{Q}\mathbf{r}^*$, the vector $\mathbf{r}$ is written in terms of $\boldsymbol{\gamma}$ by virtue of Eq. (3). It also follows from Eqs. (1) and (3) that $\dot{\boldsymbol{r}}$ can be expressed in terms of $\boldsymbol{\gamma}$ and $\boldsymbol{\omega}$ as $\dot{\mathbf{r}} = f(\boldsymbol{\gamma}, a_1, a_2)\dot{\boldsymbol{\gamma}} = f(\boldsymbol{\gamma}, a_1, a_2)(\boldsymbol{\gamma} \times \boldsymbol{\omega})$, where $f(\boldsymbol{\gamma}, a_1, a_2)$ is a certain 3×3 matrix. With allowance for Eq. (2), one can rewrite system (1) in the form of an autonomous sixth-order system of the ordinary differential equations with respect to the variables $\mathbf{M}$ and $\boldsymbol{\gamma}$.

Note that system (1) has two integrals

$$\mathcal{H} = \frac{1}{2}(\mathbf{M}, \boldsymbol{\omega}) - mg(\boldsymbol{r}, \boldsymbol{\gamma}) \;\text{ and }\; (\boldsymbol{\gamma}, \boldsymbol{\gamma}) = 1, \tag{4}$$

which are called the energy and geometric integrals, respectively. The condition $(\boldsymbol{\gamma}, \boldsymbol{\gamma}) = 1$ means that system (1) is actually five-dimensional, i.e., its phase space is $R^3 \times S^2$, since $\mathbf{M} \in R^3$ and $\boldsymbol{\gamma} \in S^2 = \{(\gamma_1, \gamma_2, \gamma_3) \big| \gamma_1^2 + \gamma_2^2 + \gamma_3^2 = 1\}$. The existence of the energy integral $\mathcal{H}$ means that the phase space is delaminated into the surfaces $\mathcal{H} = \mathrm{const}$, which are invariant with respect to the flow. Therefore, the system on each such surface is four-dimensional with the phase space that is homeomorphic to $S^2 \times S^2$.

In this case, one can elucidate a certain relation to Hamiltonian systems. However, in contrast to such systems, the nonholonomic models of the solids (including the model of Celtic stone) usually demonstrate nonconservative behavior of the trajectories at the energy levels [23]. In particular, the equilibrium states O_1 and O_2, which correspond to the so-called permanent vertical rotations whose divergences differ from zero and are opposite in sign for $0 < \delta < \pi/2$, are observed in the Celtic-stone model (1)–(3) at any energy level.

Note that system (1) is invariant with respect to the change of coordinates $\boldsymbol{\omega} \to -\boldsymbol{\omega} and \boldsymbol{\gamma} \to \boldsymbol{\gamma}$ (or, which is the same, $\mathbf{M} \to -\mathbf{M}$ and $\boldsymbol{\gamma} \to \boldsymbol{\gamma}$) and the time reversal $t \to -t$. In other words, if the time t and the angular velocities $\boldsymbol{\omega}$ are reversed in the equations of system (1), while preserving the orientation $\boldsymbol{\gamma}$, the equations acquire the previous form. Obviously, the coordinate change $h : \boldsymbol{\omega} \to -\boldsymbol{\omega}, \boldsymbol{\gamma} \to \boldsymbol{\gamma}$ is an involution, i.e., $h \circ h = \mathrm{id}$ and, therefore, system (1) is reversible. Therefore, if there exists some asymptotically stable motion Λ in the system, then a quite unstable motion $h(\Lambda)$ that is symmetric with respect to the stable motion must exist.

In many Celtic-stone models, the dynamical system has the asymptotically stable equilibrium state $O_1 : (\omega_1 = \omega_2 = \gamma_1 = \gamma_2 = 0, \gamma_3 = 1, \omega_3 = \omega_0,)$, where $\omega_0 = \sqrt{(E - mg\tilde{h})/I_3}$. This state corresponds to the vertical rotation in one direction, e.g., counterclockwise, at the corresponding level $\mathcal{H} = E$ for large energy values. Then the vertical clockwise rotation corresponds to the quite unstable equilibrium state $O_2 : (\omega_1 = \omega_2 = \gamma_1 = \gamma_2 = 0, \gamma_3 = 1, \omega_3 = -\omega_0)$. If system (1) does not have other stable limit regimes, then the trajectories of any initial point, including that specified near the unstable equilibrium state, tend to stable equilibrium. This does mean that the initial clockwise rotation of the stone should be reversed to

the stable counterclockwise rotation.

2.2. Andoyer–Deprit variables and a Poincaré map

As in many other problems of dynamics of solids, in this work the Andoyer–Deprit variables (L, H, G, g, and l), in which the condition $(\boldsymbol{\gamma}, \boldsymbol{\gamma}) = 1$ (geometrical integral) is fulfilled automatically, are rather convenient to study. These variables are defined by the following relationships [7, 9]:

$$L = M_3, \qquad G = \sqrt{M_1^2 + M_2^2 + M_3^2}, \qquad H = M_1\gamma_1 + M_2\gamma_2 + M_3\gamma_3,$$
$$l = \arg\,(M_2 + iM_1), \qquad g = \arg\,[HL/G - G\gamma_3 + i(M_2\gamma_1 - M_1\gamma_2)]. \tag{5}$$

The reverse transition is determined by the expressions

$$M_1 = \sqrt{G^2 - L^2}\sin l, \qquad M_2 = \sqrt{G^2 - L^2}\cos l, \qquad M_3 = L,$$
$$\gamma_1 = \left(\frac{H}{G}\sqrt{1 - \frac{L^2}{G^2}} + \frac{L}{G}\sqrt{1 - \frac{H^2}{G^2}}\cos g\right)\sin l + \sqrt{1 - \frac{H^2}{G^2}}\sin(g)\cos l,$$
$$\gamma_2 = \left(\frac{H}{G}\sqrt{1 - \frac{L^2}{G^2}} + \frac{L}{G}\sqrt{1 - \frac{H^2}{G^2}}\cos g\right)\cos l - \sqrt{1 - \frac{H^2}{G^2}}\sin(g)\sin l, \tag{6}$$
$$\gamma_3 = \frac{HL}{G^2} - \sqrt{1 - \frac{L^2}{G^2}}\sqrt{1 - \frac{H^2}{G^2}}\cos g. \tag{7}$$

In this work, all the graphical illustrations of numerical calculations are given for the Poincaré map of a certain global secant $\mathcal{S} = \{g = 0\}$ on which the coordinates $l, L/G$ and H/G are introduced. In these coordinates, the secant $\mathcal{S}$ can be represented as a cube $\{0 \le l < 2\pi, -1 \le L/G \le 1, -1 \le H/G \le 1\}$ for which the faces $l = 0$ and $l = 2\pi$ are identified.

3. BIFURCATIONS IN A TWO-PARAMETER FAMILY OF THE NONHOLONOMIC MODEL

In this work, we consider the nonholonomic model of Celtic stone in the form of a truncated paraboloid with the following parameters: [4]

$$I_1 = 5,\ I_2 = 6,\ I_3 = 7,\ m = 1,\ g\ = 100,\ a_1 = 9,\ a_2 = 4,\ \tilde{h} = 1. \tag{8}$$

The main bifurcations in the one-parameter families with the parameter E for the fixed angle $\delta = 0.2$ were studied in [11, 12]. In this work, we perform the two-parameter analysis in which the value of the full energy $\mathcal{H}$ (E) and the dynamic-asymmetry angle δ are considered as parameters.

Using such two-parameter families, we primarily study the stability loss bifurcations of the main regular regimes, namely, the equilibrium states and the limit cycles, and discuss the bifurcation mechanisms (scenarios) of transition to the chaotic dynamics. The main elements of the obtained bifurcation diagram on the plane of the parameters δ and E are given in Fig. 4.

This diagram shows the main bifurcation curves, i.e., the boundaries of the stability regions of the regular regimes (the curves B_1, B_2, B_3, and B_4). In this case, only the curve B_2 is a safe boundary of the stability region [24, 25] of the corresponding regime, while the other curves are unsafe boundaries. In addition, only for the bifurcation curve B_2 one can obtain its exact equation, i.e., the curve B_2 has a very simple equation $E = 1300$ in the nonholonomic model of Eqs. (1)–(3) with the stone characteristics (8). For the other curves, whose equations can be written in the form $E = B_i(\delta)$, where the functions $B_i(\delta)$ are

[4] According to the traditions of [7, 8], when introducing the dimensionless parameters, we use somewhat unusual measurement units. Thus, the linear dimensions are expressed in centimeters, time in units of $c/\sqrt{10}$, mass in kilograms (in particular, the gravitational acceleration g is assumed equal to 100 since the standard value $10\,\mathrm{m/s^2}$ is transformed to $100\,\mathrm{cm/(s/\sqrt{10})^2}$).

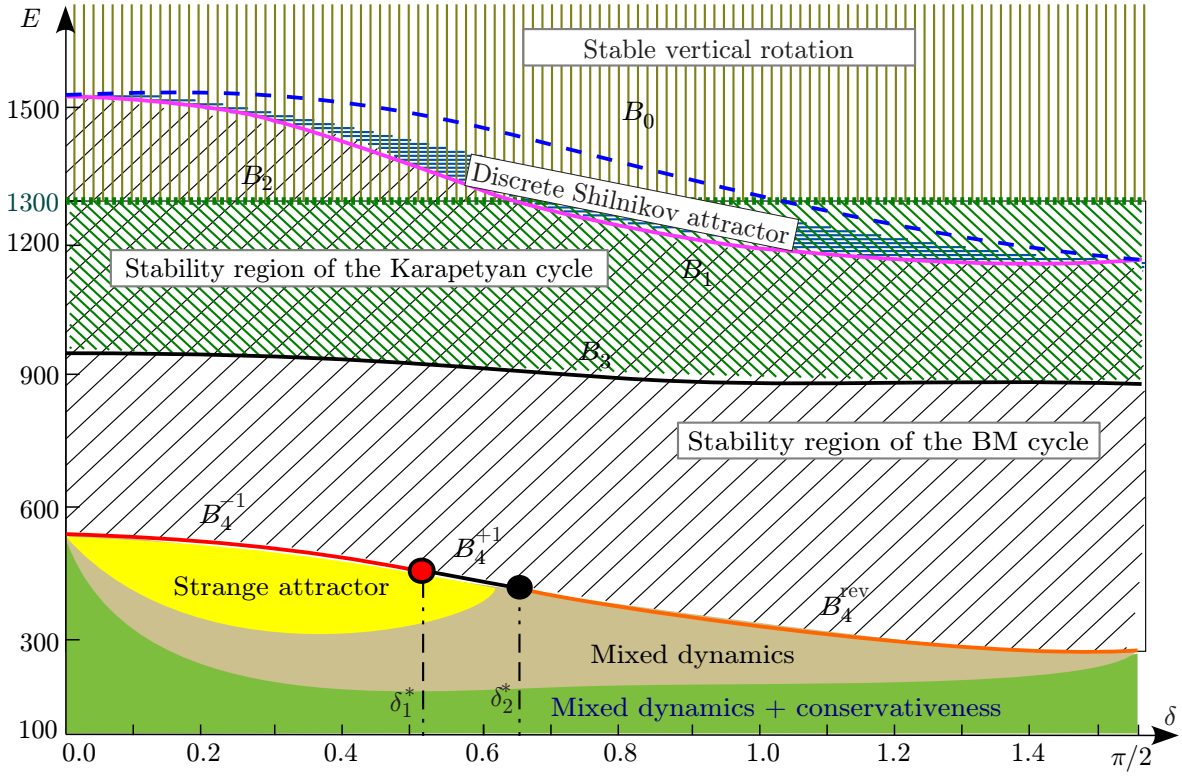

Fig. 4. Bifurcation diagram on the plane of the parameters (δ, E) for the nonholonomic stone model with the physical characteristics given by Eq. (8): B_2 is the Andronov–Hopf supercritical bifurcation (the stable limit cycle appears from the stable equilibrium state), B_1 is the Neimark–Sacker subcritical bifurcation (the saddle torus appears from the limiting cycle of the type (1,2), while the cycle itself becomes stable), B_3 and B_4^{+1} denote the saddle-node bifurcation for the limit cycles (the stable limit cycle merges with the saddle one), B_4^{-1} is the subcritical period-doubling bifurcation (the doubled-period saddle limit cycle sticks into the stable limit cycle and the saddle limit cycle appears), B_4^{rev} is the symmetric $(1, \exp(i\varphi), \exp(-i\varphi))$ bifurcation (the stable limit cycle collides with the unstable cycle on the symmetry line and both cycles disappear), B_0 is the saddle-fork bifurcation (two limit cycles of the type (1,2) merge with the symmetric limit cycle of the type (2,1) and the (1,2)-type limit cycle appears), the red dot between the curves B_4^{-1} and B_4^{+1} is the bifurcation of codimension 2 of the fold–flip type, i.e., the stable BM cycle acquires the multiplicators $(1, -1, \lambda)$ at the bifurcation time, and the black dot between the curves B_4^{+1} and B_4^{rev} is the reversible bifurcation of codimension 2 (the symmetric limit cycle with the multiplicator triad $(1, -1, 1)$) appears at the bifurcation time).

single-valued and smooth with respect to δ, their plots on the plane of the parameters δ and E are obtained numerically (using the method of parameter continuation for the corresponding stable regimes).

When studying the stable regimes in the model it is convenient to start with the simplest regime, namely, the equilibrium state O_1, which is asymptotically stable for sufficiently large E. As E decreases, the equilibrium state O_1 loses its stability on the bifurcation curve B_2 as a result of the soft (supercritical) Andronov–Hopf bifurcation. In this case, a stable limit cycle (Karapetyan cycle), which exists in the region between the curves B_2 and B_3, appears from O_1. On the curve B_3, this cycle merges with the saddle limit cycle of the same period and disappears.[5]

However, in this case, there immediately appears another regular stable regime, which was discovered for the first time in the work by Mamaev and Borisov [7] for $\delta = 0.2$ (the so-called BM cycle). The stability

[5] Symmetrically with respect to involution, the same is also observed for the quite unstable equilibrium state O_2, i.e., on the curve B_2, it gives birth to a quite unstable limit cycle, which disappears as a result of the saddle–node bifurcation on the curve B_3.

region of this limit cycle is the region between the curves B_1 and B_4. The boundary B_1 corresponds to the hard (subcritical) torus-birth bifurcation (Neimark–Sacker bifurcations), i.e., the limit cycle becomes of the saddle type (1,2) for $E > B_1(\delta)$, while it is asymptotically stable for $E < B_1(\delta)$, although giving birth to the two-dimensional saddle torus.

Note that the curve B_4 is the lower boundary of the stability region of the BM cycle and has composite structure, namely, contains the region B_4^{-1} with $0 < \delta < \delta_1^* \approx 0.52$ when the cycle acquires the multiplicator -1, the region B_4^{+1} with $\delta_1^* < \delta < \delta_2^* \approx 0.65$ when the cycle acquires the multiplicator $+1$, and the region B_4^{rev} with $\delta_2^* < \delta < \pi/2$ when the cycle becomes symmetric with respect to the involution h and its multiplicators form the triad $(+1, \exp(i\varphi), \exp(-i\varphi))$. The stability boundary B_4 is important because once it is crossed (with decreasing E), the chaotic dynamics immediately (explosively) appears in the model.

In this case, when crossing the curve B_4^{-1}, the hard (subcritical) period-doubling bifurcation is observed, i.e., the doubled-period saddle cycle sticks into the BM cycle after which the BM cycle becomes of the saddle type (2,1). Then the strange attractor, which is a spiral (flow-type) attractor since it contains the saddle-focus equilibrium state O_1, immediately appears in the model (the strange repeller, which is symmetric with respect to the strange attractor and contains the saddle-focus state O_2, simultaneously appears).

The saddle-node bifurcation with the following cycles occurs on the B_4^{+1} curve. The stable BM cycle merges with the saddle cycle of the type (2,1) and they both disappear. After that, the chaotic dynamics immediately appears, i.e., it can be either the spiral strange attractor, which contains the saddle focus O_1, or the mixed dynamics (for the angles δ which are very close to δ_2^*) of the spiral type with both saddle foci O_1 and O_2. In this case, chaos corresponding to the mixed dynamics is also certainly nonconservative since the saddle foci O_1 and O_2 have negative and positive divergences, respectively.

A reversible bifurcation (of codimension one in the case of reversible three-dimensional maps with dimension one of the line of fixed involution points $\mathrm{Fix}(h)$ [26]), which is related to the fact that the stable BM cycle merges with the quite unstable cycle that is symmetric to the BM cycle with respect to involution, occurs on the curve B_4^{rev}, and then both cycles disappear. Afterwards, the spiral-type mixed dynamics immediately becomes apparent.

Note that the chaos region $E_{\mathrm{U}} = 100 < E < B_4(\delta)$ has nonuniform structure, i.e., the strange attractor and the strange repeller that is symmetric to the attractor, which are separated from one the other, are observed in a certain parameter region adjacent to the curve B_4 (see Fig. 4). However, the mixed-dynamics region, for whose parameter values the attractor and the repeller intersect and almost coincide during the intersection, is adjacent to the above-mentioned region from below (i.e., for smaller values of E).

Finally, there exists another region corresponding to the values of E that are close to $E = E_{\mathrm{U}} = 100$, in which the mixed-dynamics regime coexists with the regime that is almost indistinguishable from the conservative one. In this case, for $E \to E_{\mathrm{U}}$, conservativeness starts to prevail, i.e., structures of the type of the Kolmogorov–Arnold–Moser (KAM) tori become more and more pronounced in this region, while the region corresponding to the mixed dynamics in the phase space becomes more and more narrow, such that it is concentrated along the separatrices of the equilibrium states O_1 and O_2 (for the Poincaré map, these lines are $W^{\mathrm{U}}(O_i) \cap S$ and $W^{\mathrm{S}}(O_i) \cap S$, where $i = 1, 2$).

3.1. Discrete Shilnikov attractor

Note that chaotic dynamics is also observed in a sufficiently narrow parameter region between the curves B_0 and B_1. This chaos is of the spiral type since the emerging attractor in the Poincaré mapping contains an immobile saddle-focus point of the type (1,2), i.e., with one-dimensional stable and two-dimensional unstable manifolds, which, in addition, intersect (see Fig. 5 showing the discrete spiral attractors for various values of δ and E). Such attractors are called the discrete Shilnikov attractors. In fact, they are discrete (for the maps) analogs of the flow-type spiral attractors containing the saddle-focus equilibrium state with a two-dimensional unstable manifold. The qualitative theory of such flow-type spiral attractors was initially

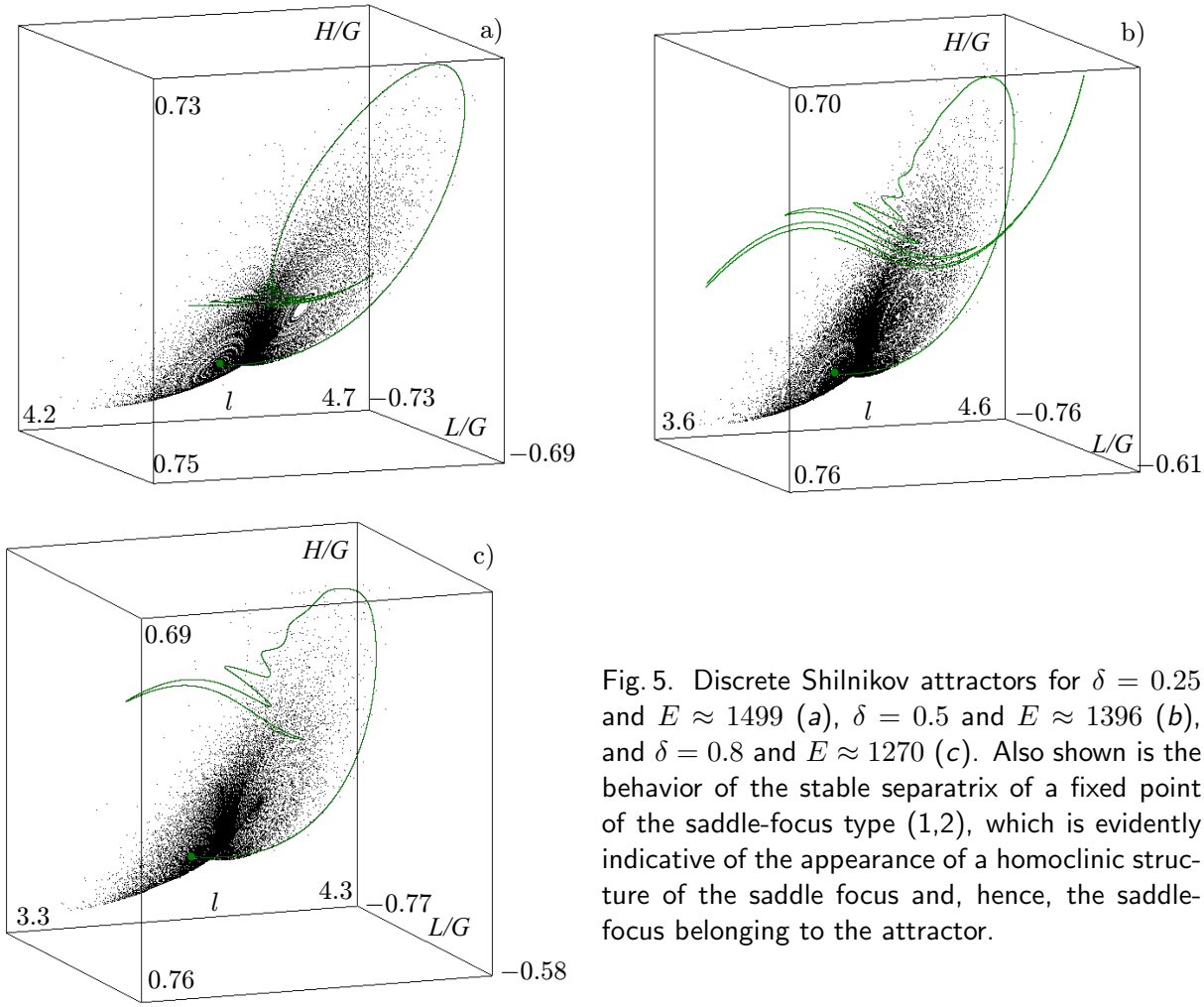

Fig. 5. Discrete Shilnikov attractors for $\delta = 0.25$ and $E \approx 1499$ (*a*), $\delta = 0.5$ and $E \approx 1396$ (*b*), and $\delta = 0.8$ and $E \approx 1270$ (*c*). Also shown is the behavior of the stable separatrix of a fixed point of the saddle-focus type (1,2), which is evidently indicative of the appearance of a homoclinic structure of the saddle focus and, hence, the saddle-focus belonging to the attractor.

developed by L. P. Shilnikov in [27]. For discrete attractors, a similar theory was proposed in [14] and also in [28–30].

In the considered model, when crossing the curve B_1 with increasing parameter E, the discrete Shilnikov attractors disintegrate as a result of the crisis caused by the appearance of heteroclinic intersections between the two-dimensional unstable manifold of the saddle focus (1,2), which is contained in the attractor, and the two-dimensional stable manifold of the saddle focus (2,1), which forms the natural boundary of the attraction region of this attractor. In any case, for $E > B_0(\delta)$, this discrete attractor is already broken and only one stable regime, namely, the equilibrium state O_1 is observed numerically. In this case, the curve B_0 corresponds to the saddle-fork bifurcation, which has codimension one due to the presence of the symmetry $l \to l + \pi$ of the Poincaré map. As a result of this bifurcation, with increasing E, two mutually symmetric saddle BM cycles of the type (1,2) merge on the curve B_0 with the symmetric saddle cycle of the type (2,1), which eventually becomes a symmetric cycle but of the type (1,2).

4. DESCRIPTION OF BIFURCATIONS IN ONE-PARAMETER FAMILIES

In this section, we present more illustrative materials for the obtained results, using the one-parameter families with the control parameter E for some fixed values of the dynamic-asymmetry angle δ (we choose three values $\delta_1 = 0.2$, $\delta_2 = 0.6$, and $\delta_3 = 1$, so that $0 < \delta_1 < \delta^* < \delta_2 < \delta^{**} < \delta_3 < \pi/2$).

The results presented in Sec. 3 are conveniently described using the so-called bifurcation trees which are shown in Figs. 6*a* and 7. In these figures, the total-energy values E and a certain characteristic coordinate

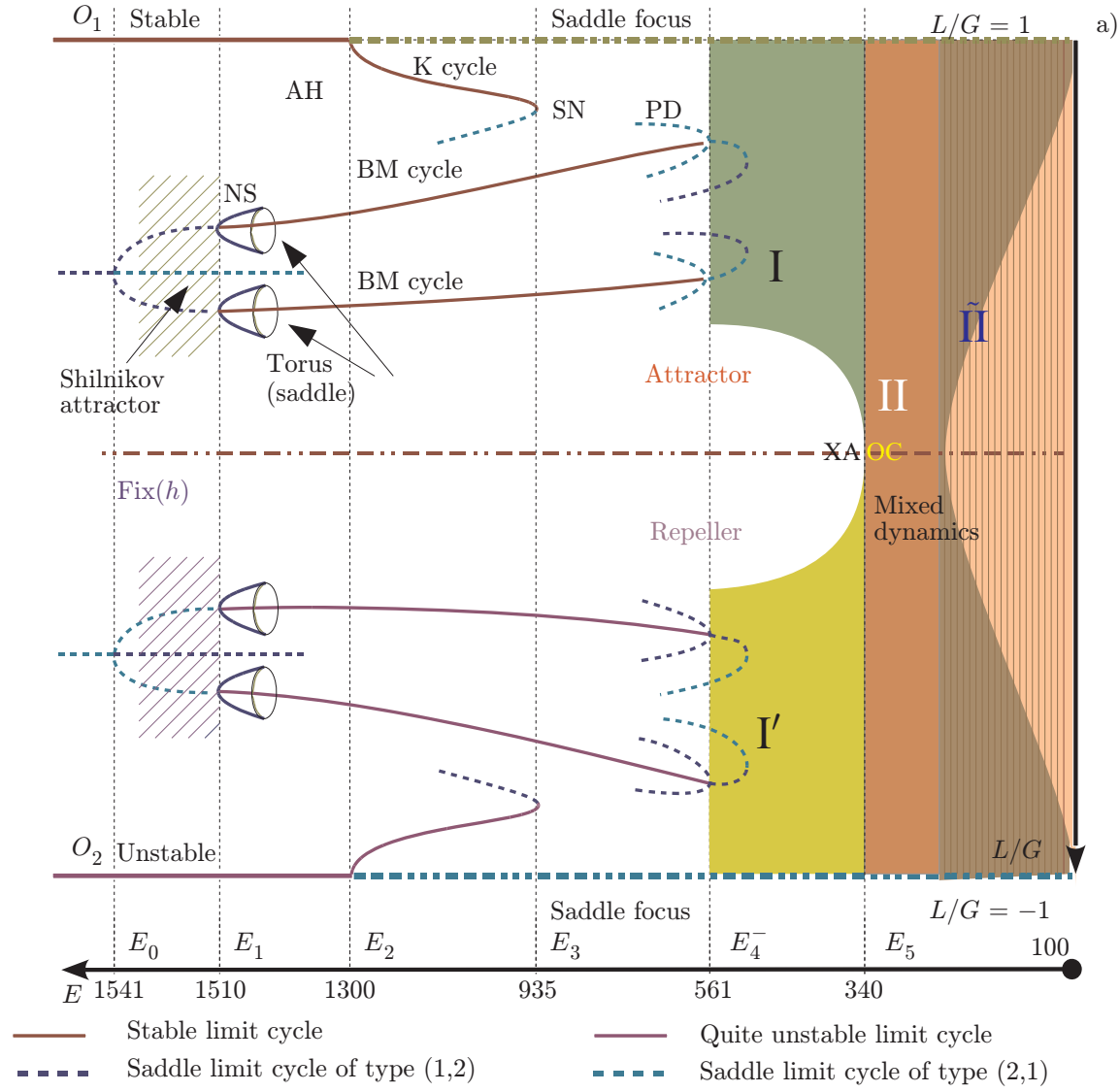

Fig. 6. The bifurcation tree for a model with $\delta = 0.2$ (*a*). Here, AH denotes the Andronov–Hopf bifurcation for the equilibrium states, while NS, SN, and PD denote the Neimark–Sacker, saddle-node, and period-doubling bifurcations for the limit cycles, respectively.

(the coordinate L/G) of the stable regime in its Poincaré map are indicated on the horizontal and vertical axes, respectively. In the case of chaotic regimes (regions I and II), the regions of variations of this coordinate from minimum to maximum values are painted. The equilibrium states O_1 and O_2 correspond to $L/G = 1$ and $L/G = -1$, respectively.

4.1. The case $\delta = 0.2$

For $E > E_2 = 1300$, the equilibrium state O_1 is asymptotically stable, while O_2 is quite unstable. For $E = E_2$, the equilibrium state O_1 loses its stability as a result of the Andronov–Hopf supercritical bifurcation, after which the stable limit cycle (the Karapetyan (K) cycle) appears in the system for $E < E_2$, and the equilibrium state O_1 becomes a saddle focus. This cycle exists up to $E = E_3 \approx 935$. For $E < E_3$, it disappears as a result of the saddle-node bifurcation upon merging with the saddle cycle of the same period.

However, there immediately appears another stable regime, namely, the BM cycle or, to be more exact, two BM cycles, which are symmetric about the plane $l = \pi$. Both cycles are asymptotically stable

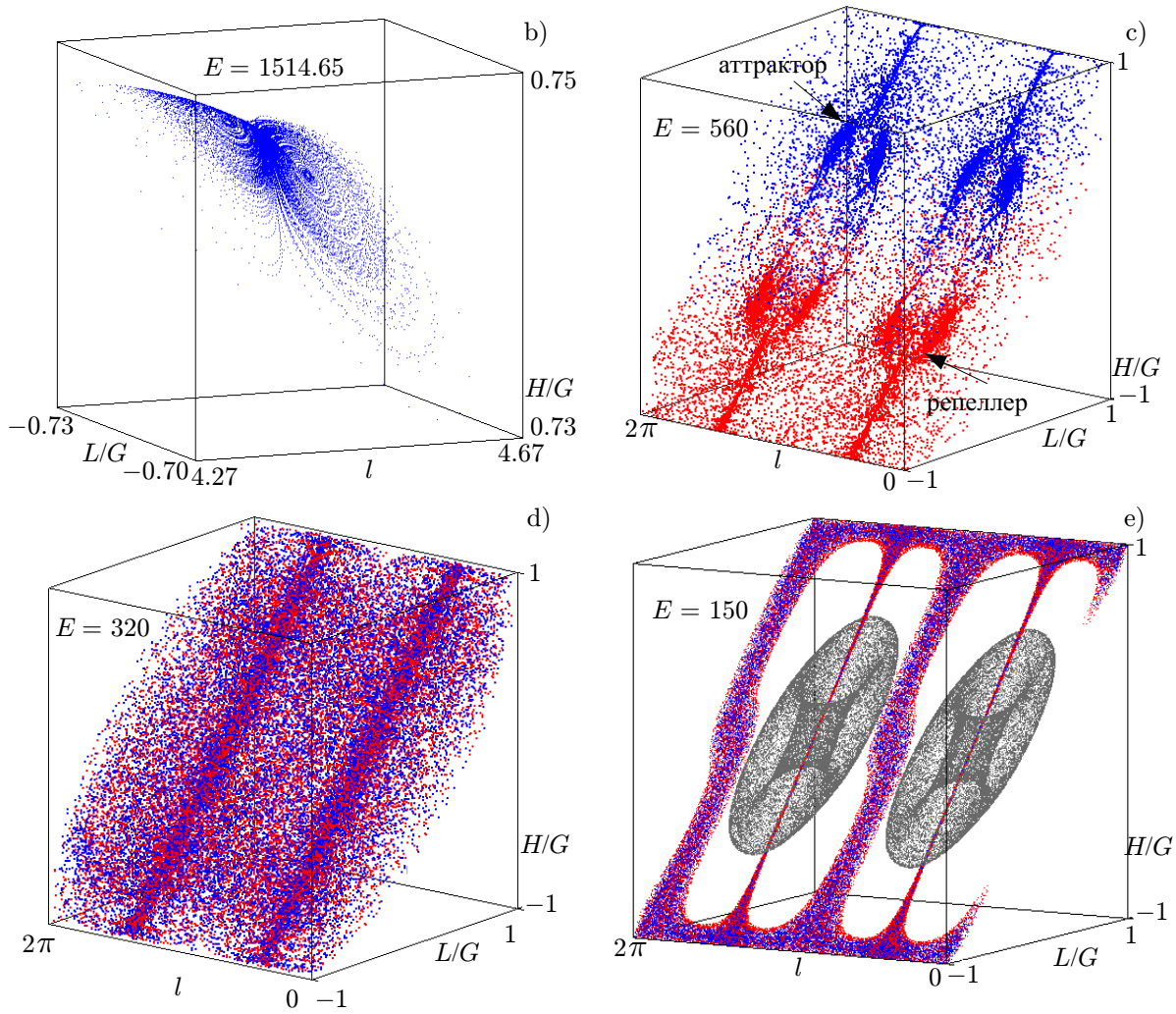

Fig. 6 (continued). The chaotic-regime portraits for the Poincaré map with the blue, red, and gray colors used to denote iterations of the points on the attractor, the repeller, and the conservative invariant sets, respectively (*b*–*e*). The discrete Shilnikov attractor is shown on panel *b*. The attractor and the repeller do not intersect on panel *c*, but almost coincide on panels *d* and *e*, so that the corresponding chaotic set (mixed dynamics) is shown, on the average, in violet tones.

for $E_4 < E < E_1$, where $E_1 \approx 1510$ and $E_4 \approx 561$. For $E > E_1$, they immediately lose stability as a result of a hard torus-birth bifurcation (subcritical Neimark–Sacker bifurcation) and become saddle foci (1,2). It is noteworthy that for the E values which slightly exceed E_1, the trajectories do not move far from these saddle foci, since they are included into a new stable regime, which is already chaotic and very quickly transforms to a discrete Shilnikov attractor (see Fig. 6*b*). This attractor exists in a very narrow interval of values of the parameter E and disappears for $E > E_0 \approx 1541$.

The line $\delta = 0.2$ intersects the curve B_4 at the point $E = E_4^- \approx 561$, which belongs to the region B_4^{-1}. Correspondingly, the spiral attractor and the spiral repeller, which is symmetric to the attractor with respect to involution, exist for $E < E_4^-$ (see Fig. 6*c*). According to the numerical calculations, for $E = E_5 \approx 340$, these attractor and repeller collide and the mixed dynamics appears (see Fig. 6*d*). However, for the E values that are very close to $E = 100$ (the region $\tilde{\Pi}$), the conservative chaotic dynamics is also observed. In this case, according to the numerical simulation results, it is very similar to the Hamiltonian dynamics, which is close to the integrable one and may have invariant sets that are similar to the KAM tori (see Fig. 6*e*).

4.2. The cases $\delta = 0.6$ and $\delta = 1$

By analogy with Fig. 6, Fig. 7 shows bifurcation trees for the model if $\delta = 0.6$, where $\delta_1^* < \delta < \delta_2^*$ (panel *a*), and $\delta = 1 > \delta_2^*$ (panel *b*). According to Sec. 3, in these cases, the bifurcations observed during the intersection of the curves B_0, B_1, B_2, and B_3 do not differ from those in the case $\delta = 0.2$, but occur for somewhat different values of the energy E (see Fig. 7). However, as is evident from Fig. 4, for $\delta > \hat{\delta} \approx 0.68$, the sequence of these bifurcations can vary, i.e., in this case, the curves B_1 and B_2 intersect for $\delta = \hat{\delta}$. However, when crossing the line B_4, the bifurcations change.

The line $\delta = 0.6$ intersects the bifurcation curve B_4 at the point $E = E_4^+ \approx 458$, which belongs to the region B_4^{+1}. In this case, the stable BM cycle disappears as a result of the saddle-node bifurcation (the same occurs with a quite unstable cycle). Once $E < E_4^+$, the spiral attractor and (for inverse iterations) the spiral repeller appear. They exist in a sufficiently narrow interval of values of the parameter E (the regions I and I′ in Fig. 7*a*). For $E \approx 463$, the spiral attractor and the spiral repeller collide and the mixed dynamics appears (regions II in Fig. 7*a*).

In the case $\delta = 1$, the stable (and also unstable) BM cycles reach the symmetry line $L/G = H/G = 0$ on which they collide and disappear at $E = E_4^r \approx 363$ as a result of a reversible bifurcation that is related to the appearance of the multiplicators $+1$, $\exp(i\varphi)$ and $\exp(-i\varphi)$ of the symmetric point [26]. Note that the coordinates of intersection of these cycles with the secant $S = 0$ along the axes L/G and H/G ($L/G = H/G = 0$) coincide, while they differ by π when intersection takes place along the l axis. In this case, for $E < E_4^r$, there immediately appears the spiral mixed dynamics containing both saddle foci O_1 and O_2.

Since the phase portraits for both $\delta = 0.6$ and $\delta = 1$ for various values of the parameter-E differ only slightly from the corresponding phase portraits in the case $\delta = 0.2$, which are shown in Figs. 6*a*, 6*c*, and 6*d*, they are not considered in this work.

Note that the regions $\tilde{\text{II}}$ in Figs. 6 and 7 have a double color. The dark-brown color of the background and shading mean that the coordinate L/G of the points of such a chaotic regime as mixed dynamics has a range from -1 to $+1$. The light-brown background refers to the conservativeness regime and reflects the fact that the coordinate L/G of the points on it varies within the limited range, which is symmetric with respect to the ratio $L/G = 0$ and increases when approaching $E = 100$.

5. MULTISTABILITY OF A NONHOLONOMIC MODEL

One of the most interesting properties of the Celtic-stone dynamics as well as many other nonholonomic models is multistability, which is manifested in that different-type stable regimes can coexist in the phase space for the same parameter values (see, e.g., [7, 9, 15]).

It is evident from the bifurcation diagram for the nonholonomic model (8) of the stone in Fig. 4 that the plane of the parameters δ and E has the regions with monostable dynamics. There also exist the regions in which the corresponding system is multistable according to the results of numerical experiments. First, it is the region of parameters above the curves $E = B_0(\delta)$ and $E = B_2(\delta)$, in which the equilibrium state O_1 is the only stable regime. Second, it is the region $B_0(\delta) < E < B_2(\delta)$, in which the Karapetyan cycle is the only stable regime. We can also mention the regions denoted as the strange attractor and the mixed dynamics in which multistability is not observed, at least, in numerical experiments, although various stable periodic trajectories of rather large periods can also exist in this case [31].

In the other regions, multistability is observed. For example, the region corresponding to the discrete Shilnikov attractor intersects with the regions of existence of the stable equilibrium state O_1 and the region of the Karapetyan-cycle existence. The latter also intersects with the region of existence of the stable BM cycle, i.e., the Karapetyan cycle and two stable BM cycles coexist in the region $\{B_3(\delta) < E < B_2(\delta\} \cap \{B_3(\delta) < E < B_1(\delta\})$. The region $B_3(\delta) < E < B_4(\delta)$ has two stable BM cycles. Finally, another unusual multistability type where the mixed dynamics and KAM structures coexist is observed in the mixed dynamics + conservativeness region.

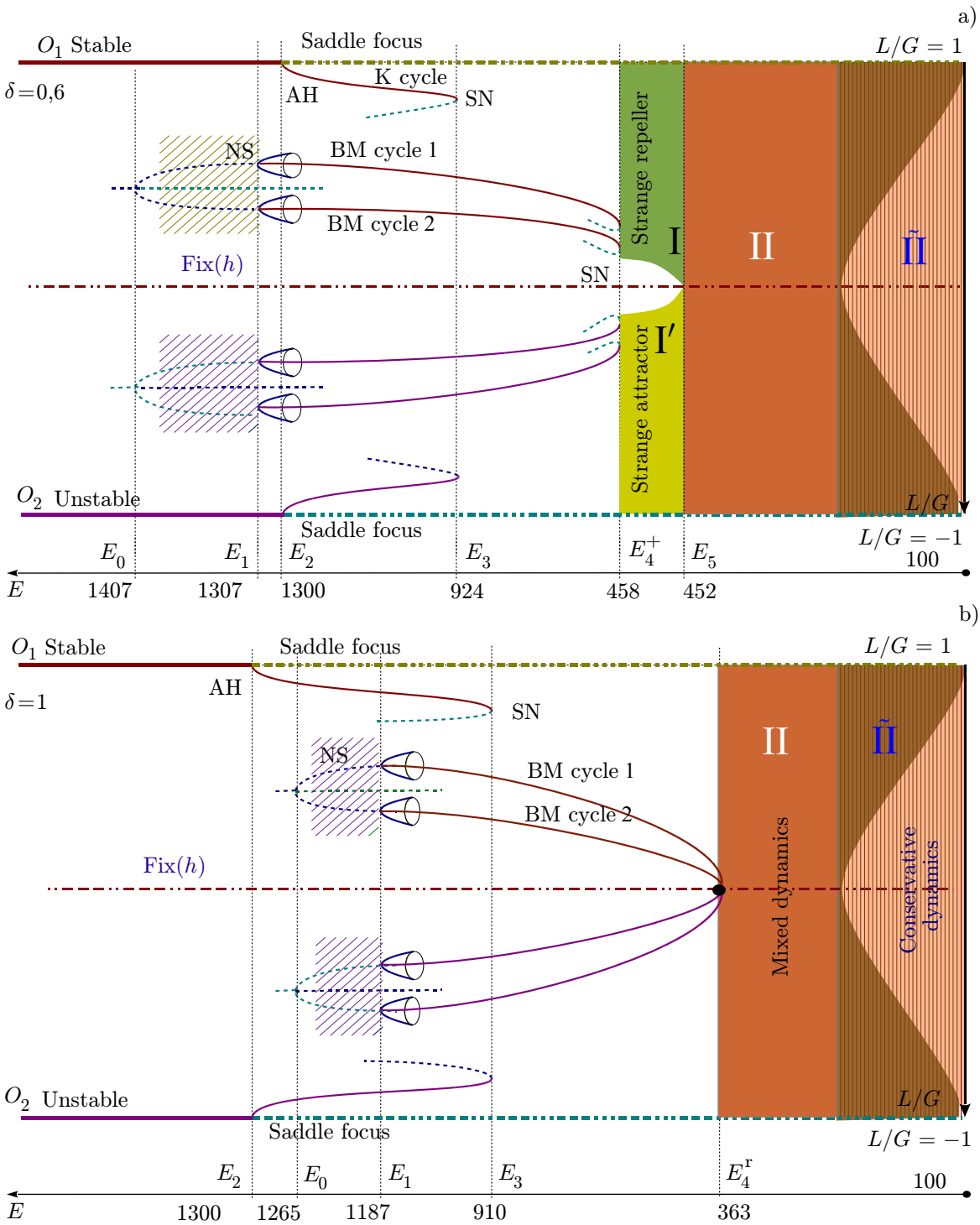

Fig. 7. Bifurcation tree for the model at $\delta = 0.6$ (*a*) and $\delta = 1$ (*b*). On panel *a*, the BM cycle loses its stability on the curve B_4^+ as a result of the saddle-node bifurcation after which one can observe the spiral attractor, which contains the saddle focus O_1, and the spiral repeller, which contains the saddle focus O_2. On panel *b*, the BM cycle loses its stability on the curve B_4^{rev} as a result of the reversible bifurcation $+1, \exp(i\varphi), \exp(-i\varphi)$, i.e., it collides with the quite unstable BM cycle, which is symmetric to it with respect to involution, and they both disappear after which the mixed dynamics hardly appears.

6. CONCLUSIONS

The following main results of this work can be emphasized: (i) the parameter regions corresponding to the existence of the discrete Shilnikov attractors (see Figs. 5 and 6*b*) have been found;

(ii) new bifurcation mechanisms (scenarios) of transition to chaos, namely, strange attractors and mixed dynamics, have been established and studied;

(iii) a new scenario of transition to chaos (mixed dynamics) as a result of the collision of stable and quite unstable limit cycles, which are symmetric with respect to involution, has been found;

(iv) a bifurcation diagram (see Fig. 4) showing the boundary (the bifurcation curve B_4) between the parameters ranges corresponduing to the regular and chaotic dynamics, has been developed on the parameters plane (δ, E);

(v) on the bifurcation diagram, the regions of multistability have been found and its types have been described.

The studies of the dynamics of the nonholonomic models of a Celtic stone, which have been performed in recent years, confirm the empirical fact that this dynamics can be extremely complicated and diverse. Using numerical methods along with modern approaches of the qualitative theory and the bifurcation theory allows one to obtain rather informative and interesting results, which go far beyond the scope of the problem of studying the Celtic-stone dynamics. They reveal new dynamic phenomena which may be observed in multidimensional models.

Mixed dynamics is one of such recently discovered phenomena. Actually, the nonholonomic model of a Celtic stone is the first applied model in which this phenomenon was discovered [12]. This discovery has caused significant interest in studying other models including those describing the solid dynamics to obtain information on bifurcations and mixed dynamics which are realized in these models.

The issues of bifurcation scenarios of the mixed-dynamics emergence in the nonholonomic model of a Celtic stone have also been considered in this work. In particular, we have found a rather simple scenario related to the "explosive" transition to the mixed dynamics as a result of a reversible bifurcation of collision of the periodic sink and the source on the bifurcation curve B_4. We have shown that this stability-loss curve of the regular regime consists of three parts corresponding to bifurcations of various types. Definitely, its complete bifurcation analysis with the development of the corresponding bifurcation diagram and description of the phase-trajectory rearrangements is one of the most important and obvious problems in this field, which will be analyzed by the authors of this work in the nearest future. The issues which also seem to be very interesting and can determine new and rather promising lines of studies are as follows. Are the bifurcation scenarios considered in this work characteristic of the majority of nonholonomic models? What new features of the stability-loss bifurcations can be expected in these models in view of the fact that in particular the discrete Lorenz attractor was found in a Celtic-stone model [12]? What is the structure of chaotic regimes, including the mixed-dynamics regime?

We thank D. V. Turaev for useful comments. This work was performed within the framework of the grant of the Russian Science Foundation (project No. 14–12–00811). We thank the Russian Foundation for Basic Research (project Nos. 18–29–10081, 18–31–20052, and 18–31–00431) and the Ministry of Education and Science of the Russian Federation (project No. 1.3287.2017) for support. A. Kazakov and E. Samylina acknowledge the support from the Fundamental Research Program of the National Research University "Higher School of Economics" for 2018. The studies of Sec. 3.1 and 4.1 were performed within the framework of the grant of the Russian Science Foundation (project No. 18–71–00127).

REFERENCES

1. A. S. Gonchenko and A. O. Kazakov, "Secrets of the Celtic-stone dynamics," in: *Nauchn. Obozr.*, No. 2 (12), 14 (2012).
2. G. T. Walker, *Proc. Cambridge Philos. Soc.*, **8**, 305 (1895).

3. J. Walker, *Sci. Am.*, **241**, 172 (1979).
4. I. S. Astapov, *Vest. Moscow State Univ., Matem. Mekh.*, No. 2, 97 (1980).
5. A. V. Karapetyan, *Prikl. Mat. Mekh.*, **45**, No. 5, 808 (1981).
6. A. P. Markeev, *Prikl. Mat. Mekh.*, **47**, No. 4, 575 (1983).
7. A. V. Borisov and I. S. Mamaev, *Physics — Uspekhi*, **46**, No. 4, 393 (2003).
8. A. V. Borisov, A. A. Kilin, and I. S. Mamaev, *Doklady Physics*, **51**, No. 5, 272 (2006).
9. S. P. Kuznetsov, A. Yu. Zhalnin, I. R. Sataev, and Yu. V. Sedova, *Nelin. Din.*, **8**, No. 4, 735 (2012).
10. A. V. Borisov, A. O. Kazakov, and S. P. Kuznetsov, *Physics — Uspekhi*, **57**, No. 5, 453 (2014).
11. A. S. Gonchenko, S. V. Gonchenko, and A. O. Kazakov, *Nelin. Din.*, **8**, No. 3, 507 (2012).
12. A. S. Gonchenko, S. V. Gonchenko, and A. O. Kazakov, *Reg. Chaot. Dyn.*, **18**, No. 5, 521 (2013).
13. S. V. Gonchenko, I. I. Ovsyannikov, C. Simo, and D. Turaev, *Int. J. Bifur. Chaos*, **15**, No. 11, 3493 (2005).
14. A. S. Gonchenko, S. V. Gonchenko, and L. P. Shilnikov, *Nonlin. Din.*, **8**, No. 1, 3 (2012).
15. A. V. Borisov, A. O. Kazakov, and I. R. Sataev, *Reg. Chaot. Dyn.*, **19**, No. 6, 718 (2014).
16. S. V. Gonchenko and D. V. Turaev, *Proc. Steklov. Inst. Math.*, **297**, No. 1, 116 (2017).
17. S. Gonchenko, *Discont. Nonlin. Complex.*, **5**, No. 4, 365 (2016).
18. A. S. Gonchenko, S. V. Gonchenko, A. O. Kazakov, and D. V. Turaev, *Physica D*, **350**, 45 (2017).
19. A. O. Kazakov, arXiv:1801.00150.[math.DS] (2017).
20. A. O. Kazakov, *Reg. Chaot. Dyn.*, **18**, No. 5, 508 (2013).
21. S. P. Kuznetsov, *Europhys. Lett.*, **118**, No. 1, 10007 (2017).
22. S. P. Kuznetsov, *Reg. Chaot. Dyn.*, **23**, No. 2, 178 (2018).
23. V. V. Kozlov, *Usp. Mekh.*, **8**, No. 3, 85 (1985).
24. N. N. Bautin, *Behavior of Dynamical Systems near the Stability Region Boundaries* [in Russian], Nauka, Moscow (1984).
25. N. N. Bautin and L. P. Shilnikov, Supplement I to: J. E. Marsden and M. McCracken, *The Hopf Bifurcation and its Applications*, Springer-Verlag, New York (1976).
26. L. M. Lerman and D. Turaev, *Reg. Chaot. Dyn.*, **17**, Nos. 3–4, 318 (2012).
27. L. P. Shilnikov, in: *Methods of Qualitative Theory of Differential Equations* [in Russian], Gorky (1986), p. 150.
28. A. S. Gonchenko, S. V. Gonchenko, A. O. Kazakov, and D. Turaev, *Int. J. Bifur. Chaos*, **24**, No. 8, 1440005 (2014).
29. A. S. Gonchenko and S. V. Gonchenko, *Physica D*, **337**, 43 (2016).
30. A. V. Borisov, A. O. Kazakov, and I. R. Sataev, *Reg. Chaot. Dyn.*, **21**, Nos. 7–8, 939 (2016).
31. V. S. Afraimovich and L. P. Shilnikov, "Strange attractors and quasiattractors," in: G. I. Barenblatt, G. Iooss, and D. D. Joseph, eds., *Nonlinear Dynamics and Turbulence*, Pitmen, Boston (1983), p. 1.